Lattice Dynamics in Hydrogenated Austenitic Stainless Steels and in the Superionic Conductor $Cu_{2-\delta}Se$

Dr. rer. nat. Thesis
by
Dipl.-Phys. Vedran Rajevac
from
Zagreb, Croatia

Fachbereich Material- und Geowissenschaften
Fachgebiet Strukturforschung

Technische Universität Darmstadt

Referent: Prof. Dr. Hartmut Fueß
Koreferent: Prof. Dr. Hermann Rauh
Tag der Einreichung: 6. Juli 2004
Tag der mündlichen Prüfung: 6. August 2004

Darmstadt, 2004
D17

Acknowledgements

Thanks to all working group especially to: Victor Joco, Dr. Alexander Morlang, Jean-Christophe Jaud, Björn Schwarz for support and help during my PhD thesis.

Thanks to my mother for support during all my education especially during my stay in Germany.

Contents

Chapter 1

Introduction

The objects of research are lattice dynamics in face centred cubic(fcc) systems; austenitic stainless steels, hydrogenated austenitic stainless steels and superionic conductor $Cu_{2-\delta}Se$. The task can be divided into three parts: modelling of lattice dynamics in austenitic stainless steels with different composition; modelling of optic hydrogen vibrations in austenitic stainless steels with variations in alloying composition and hydrogen contents; investigation of structure and lattice dynamics of copper selenide $Cu_{2-x}Se$ compounds with different compositions.

Austenitic stainless steels are widely used because they combine high corrosion resistance with excellent mechanical and physical properties. They are used in the chemical industry, oil refining, food production, energy production, medicine and naval transport. These properties can be tuned by variation of the composition of the main elements Fe, Cr and Ni, by adding further alloying elements and also by changes in their microstructure due to thermal and mechanical treatment. To design a steel for a distinct application, a prediction of its properties based on its chemical composition would be supportive. The effects of alloying additions on the engineering elastic moduli of austenitic stainless steels have been investigated by ultrasonic measurements [Ledbetter 1985, Ledbetter 1988, Kim 1994] and inelastic neutron scattering [Beskrovni 1999]. As an example, it was found that adding Ni as well as Cr (both as substitute for Fe) leads to an increase in the bulk modulus accompanied by a decrease in the shear modulus [Kim 1994]. These results contradict predictions based on the theory of elasticity, as substituting Fe with Cr leads to a lattice expansion while substituting Fe with Ni decreases the lattice parameter. Furthermore, it is remarkable that bulk modulus and shear modulus change in opposite directions. These results indicate significant changes in the interatomic bonding due to modifications in the chemical composition in such a way, that dilatational modes and shear modes are affected in a quite different manner. Recently, the effects of alloying additions on the properties of austenitic stainless steels have been derived from ab-initio quantum mechanical calculations [Vitos 2003].

Phonon dispersion curves are often used to verify interatomic potentials. Inelastic neutron scattering is the only method for the determination of phonon dispersion relations in a broad range of momentum transfer from low q limit till the edge of the Brillouin zone.

Moreover, semi-empirical approaches, such as the embedded-atom method, require elastic constants and characteristic points in the phonon dispersion curves among the parameters for the determination of interatomic potentials, from which the material properties can be derived.

In previous studies, the phonon dispersion branches L-[110] and T_1-[110] of Fe-18Cr-16Ni-10Mn steel, measured with time-of-flight neutron spectroscopy [Danilkin 1997], and the low q regions of the phonon dispersion branches, measured with triple-axis neutron spectroscopy [Danilkin 2001], have been presented. Also, the phonon dispersion branches of Fe-18Cr-12Ni-2Mo were measured along the symmetry directions [100], [110] and [111] [Hoelzel 2002].

Interstitial impurity like hydrogen, nitrogen and carbon have great impact on the mechanical properties of austenitic stainless steels. Interstitial hydrogen leads to softening of acoustic phonon modes which is a sign of phase transition. Investigation of lattice dynamics is important because it allows to predict in which condition phase transition occur and what is the influence of hydrogen on the mechanical properties of austenitic stainless steels.

Metal atoms in austenitic stainless steels build fcc lattice. As experimental method inelastic neutron scattering on single crystal as well as on polycrystalline samples were used. On single crystal data was performed firstly very simple Born-von Karman model and later slightly more sophisticated corrections based on the influence of the electron gas on lattice dynamics. From these models force constants were obtained which gave information about average bonding between atoms. From force constants phonon dispersion curves were derived in arbitrary direction and phonon density of states. Obtained phonon density of states was compared with experimental data. From experimental data for phonon density of states, thermal properties of the system were derived. To my knowledge no studies about thermal properties like heat capacity or internal energy in low temperature region in austenitic stainless steels exist. The derived values of mean square displacement were compared with diffraction studies.

From the knowledge of lattice dynamics in non-hydrogenated austenitic stainless steels next step is to investigate influence of hydrogenation on the interatomic potential. From the knowledge of interatomic potential it is possible to predict mechanical properties as well as parameters of phase transition on hydrogenated austenitic stainless steels. The previous study [Hoelzel 2004] gave information about the phase diagram of austenitic stainless steels under the hydrogenation and high pressure treatment. Phase transition is connected with hydrogen embrittlement. In this study information about interatomic potential from performed modelling of hydrogen modes in austenitic stainless steels is obtained. Result of modelling are compared with experimental data for hydrogen modes.

Hydrogenation was performed by high pressure treatment to gain homogenous distribution of hydrogen and to minimise internal stresses. In austenitic stainless steels diffraction and inelastic neutron scattering were performed on samples with low (H/Me≪0.1), medium (0.1<H/Me<0.9) and high (H/Me>0.9) hydrogen content. Diffraction studies gave information about phase stability and also about distribution of hydrogen in the unit cell. From the results of diffraction studies and from INS studies on a fully hydrogenated system a

simple model was derived which takes into account the influence on hydrogen-hydrogen bonding as well as the influence of different alloying elements in austenitic stainless steels. This model was applied on fully hydrogenated austenitic stainless steels. By a fitting procedure force constants H-H were obtained. From these data modelling of phonon densities of states in medium and low hydrogen contained samples were performed. Derived values for phonon density of states were compared with experimental data.

In the second part of this thesis investigations on $Cu_{2-\delta}Se$ systems were performed. A special class of ionic solids, so called superionics, have values of electrical conductivity in the solid state similar to those of molten solids. Mobility of ions is responsible for this effect. This property makes superionic conductors suitable for energy storage devices [Hooper 1978]. The conduction mechanism of the fast ion conductors is complex and is not fully elucidated at present.

Copper selenide is of great interest from theoretical and technological point of view due to its superionic conductivity. The superionic(α) phase adopts fcc structure. Selenium atoms build sublattice and copper atoms are distributed over a number of vacant interstitial sites [Rahlfs 1936]. The simple structure of the selenium sublattice makes this compound attractive as a model system for the investigation of diffusion and disordering processes.
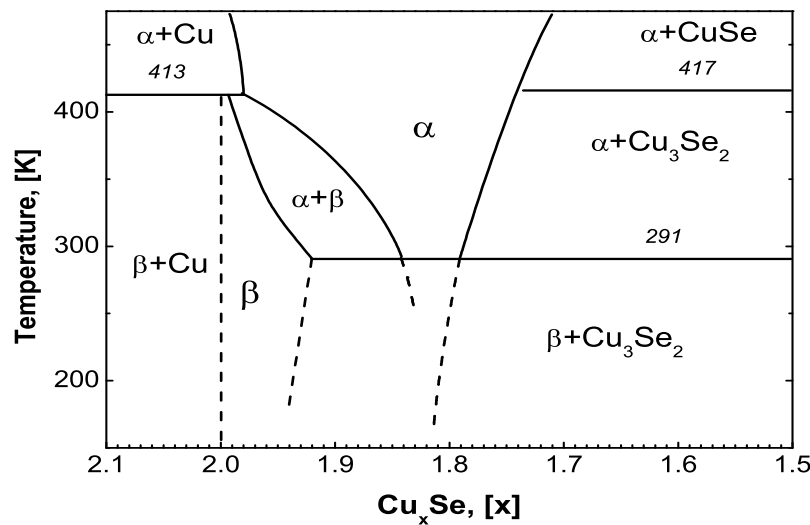
Figure 1.1: The phase diagram for copper selenide system.

$Cu_{2-\delta}Se$ exists in two modifications: the low-temperature β-phase and the high-temperature α-phase. The α-phase has a wide homogeneity region, $0.02 < \delta < 0.29$ at T = 414 K, and its electro-physical properties vary strongly with composition within this range [Abrikosov 1983, Yakshibaev 1984, Korzhuev 1989]. The $\beta \rightarrow \alpha$ phase transition temperature is 414 K [fig. 1.1] in Cu_2Se and decreases with increasing δ. Ionic conductivity of β-Cu_2Se at room temperature is about 0.01 $\Omega^{-1}cm^{-1}$ and in α-$Cu_{1.75}Se$ [Yakshibaev 1984, Korzhuev 1989] one

order of magnitude higher. In α-Cu_2Se the conductivity reaches values of 1-2 $\Omega^{-1}cm^{-1}$ - which is several times higher than in $Cu_{1.75}Se$ in the temperature range of around 500K. The aim of the structural studies was the determination of the origin of the ionic disorder. From the structural studies information about the phase diagram are obtained. One of the aim of the studies is the influence of ionic conductivity on lattice dynamics, which is especially pronounced in the low-energy mode.

Based on the literature data about ionic motion, mechanism of conduction [Rahlfs 1936, Heyding 1976, Yamamoto 1991, Sakuma 1989, Boyce 1981, Oliveria 1988] could be obtained. It is well establish that the α-phase has Fm$\overline{3}$m symmetry with selenium atoms in Wyckoff 4a position. Reported distributions on copper ions are rather controversial. Quite complicated models for copper ion distribution over 8c and 32f sites have been reported in [Heyding 1976, Yamamoto 1991, Sakuma 1989, Sakuma 1995] based on X-ray and neutron diffraction studies. According to [Oliveria 1988] all copper atoms have only one equilibrium position in 32f sites within tetrahedral voids. No copper density has been observed in octahedral voids in [Boyce 1981]. This result [Boyce 1981, Oliveria 1988] indicates the most probable drift pathway of diffusion for copper ions from the center of tetrahedra to the center of neighbouring tetrahedra [Koto 1980]. While the results of [Boyce 1981, Oliveria 1988] with no copper atoms in octahedra for α-$Cu_{2-\delta}Se$ could not explain ionic conductivity well. Reports on the structure of the β-phase are even more controversial[Milat 1987]. Different crystallographic data [Milat 1987b] were reported for β-$Cu_{2-\delta}Se$. Most reliable studies on β-$Cu_{2-\delta}Se$ show that the structure of Cu_2Se at room temperature is monoclinic with a unit cell of space group Cm and cell parameters: $a_m = $ 7.115(5) Å, $b_m = $ 12.34(1) Å, $c_m = $ 7.119(5) Å, $\beta_m = $ 108.0(4)° and with possible space group Cm [Milat 1987]. The study [Milat 1987] was based on single crystal X-ray diffraction data and transmission electron microscopy.

It is assumed that transport properties in copper selenide are correlated with lattice dynamics [Salamon 1979]. This is especially pronounced for the low-energy (LE) mode of superionic conductors and the damping of phonon modes. It is a dispersionless mode with typical energy of excitation of 2-5 meV. The physical background of low energy mode are still under debate, but the most common explanation is a localised mode characteristic for highly disordered systems. Recently, Wakamura proposed a correlation between the frequency of the LE-mode and the activation energy of self-diffusion [Yamamoto 1991]. LE modes in copper selenide were observed by Sakuma [Sakuma 1989] in inelastic neutron scattering studies. In the diffraction part were investigated phase analysis due to influence of the composition and temperature. This study gave additional information about distribution of copper atoms which is essential for understanding of the diffusion process. In the high temperature region a strong indication of a copper releasing process occurs. In these systems also investigations on lattice dynamics by INS as well as the influence of composition and temperature were performed.

Chapter 2

Theoretical background

2.1   Lattice dynamics on discrete systems

The duality of waves and particles is a basic concept of quantum physics. Many properties in solids show wave and particle aspects depending on the experiment performed. One application of this concept is the description of lattice vibrations which can be treated as waves as well as particles. For a better understanding of the physical nature of the crystal a concept of interaction between particles is necessary to introduce. Basically, short and long range interactions exist. In this work the influence of the short range interaction on lattice dynamics will mostly be discussed.

An ideal crystal system is defined by a discrete translational symmetry, repeated to infinity and a interatomic potential was introduced, in the way that particles(atoms, ions) are located in the stable equilibrium. The Hamiltonian H of the crystal system has then the form [Willis 1975]:

$$H = \frac{1}{2} \sum_{i,j} \left(\frac{\vec{p}_{i,j}^2}{2m_{ij}} + V(r_{i,j}) \right), \qquad (2.1)$$

where the summation is over all atomic positions. In the case of an analytic function for the potential energy the Taylor expansion is possible. In the investigations on lattice dynamics, a Taylor expansion is performed around the minimum point [Willis 1975] of the lattice potential:

$$V = V_0 + \sum_{k,\alpha} \left(\frac{\partial V}{\partial u_\alpha(k)} \right)_0 u_\alpha(k) + \frac{1}{2} \sum_{k,k',\alpha,\alpha'} \left(\frac{\partial^2 V}{\partial u_\alpha(k) \partial u_{\alpha'}(k')} \right)_0 u_\alpha(k) u_{\alpha'}(k') + ... \qquad (2.2)$$

Index "0" means, that the derivations were calculated in the equilibrium point of the potential. In this relation, k defines the atomic positions of the atoms and α the component of the displacement in the given coordinate system. In the expansion, the zero term is defined by the zero point in the potential. The value of the minimum of the potential is not important for the investigations on lattice dynamics. The linear terms in the displacements are zero because of the condition, that the potential is expanded around its minimum; so

all important physical properties are described by second and higher order terms. In the major part of this thesis, only harmonic approximation will mainly be applied. Using a Taylor expansion the force matrix [Willis 1975] was obtained:

$$\Phi_{\alpha\alpha'}(kk') = \left(\frac{\partial^2 V}{\partial u_\alpha(k) \partial u_{\alpha'}(k')} \right)_0, \tag{2.3}$$

which describes the force constants. In this work the formalism of the dynamical matrix will be used [Willis 1975], which is defined by:

$$D_{\alpha,\alpha'}(kk' \mid \vec{q}) = \frac{1}{\sqrt{m_k m'_k}} \sum_{l'} \Phi_{\alpha,\alpha'} \begin{pmatrix} k & k' \\ 0 & l' \end{pmatrix} \exp\left[i\vec{q}(\vec{r}(k'l') - \vec{r}(k0)) \right]. \tag{2.4}$$

In this formalism the harmonic part of the potential can be written in the form:

$$V = \frac{1}{2} \sum_{k,k',\alpha,\alpha'} \Phi_{\alpha,\alpha'} \begin{pmatrix} k & k' \\ l & l' \end{pmatrix} u_\alpha(k) u_{\alpha'}(k'). \tag{2.5}$$

Which with the Hamiltonian equations of motion:

$$\dot{\vec{q}}_{ij} = \frac{\partial H}{\partial \dot{\vec{p}}_{ij}} \tag{2.6}$$

$$\dot{\vec{p}}_{ij} = -\frac{\partial H}{\partial \dot{\vec{q}}_{ij}} \tag{2.7}$$

leads to the definition of the force matrix:

$$\vec{F}(k) = -\Phi(k,k')\vec{u}(k') \tag{2.8}$$

where are $\Phi(k, k')$ 3×3 force matrix. From relations(eq. 2.3, 2.8) equations of motion are obtained:

$$\ddot{u}_\alpha(k,t) = -\sum_{k',\alpha'} \Phi_{\alpha,\alpha'} \begin{pmatrix} k & k' \\ l & l' \end{pmatrix} u_{\alpha'}(k',t). \tag{2.9}$$

The equations of motion are linear, thus the principle of superposition is valid. In this case the solution of the equation of motions can be written as a linear combination of plane waves:

$$u(\vec{k},t) = A(\vec{k})\vec{e}(\vec{k})e^{i(\vec{k}\vec{r}-\omega t)}. \tag{2.10}$$

Where $A(k)$ is the amplitude, $\vec{e}(k)$ the polarization vector and $e^{-i\omega t}$ is the time dependent part of the plane wave.

The dynamical matrix is real and symmetrical for all potentials that can be represented by analytical functions. From this properties of the dynamical matrix it follows that its eigenvalues are real and by a diagonalisation of the dynamical matrix phonon dispersion curves can be derived. The dynamical matrix depends on the symmetry of the system.

The dimension of the dynamical matrix is equal to 3N×3N, where N is the number of atoms in the basis. In a monoatomic system only acoustic modes exist. In this case, one longitudinal and two transversal modes of vibrations exist. With higher number of atoms in the unit cell optic modes appear. From the phonon dispersion curves the phonon density of states in all directions can be derived using the relation:

$$g(\omega) = \sum_s \int_S \frac{d\vec{S}}{(2\pi)^3} \frac{1}{|\vec{\nabla}\omega_s(\vec{k})|}. \tag{2.11}$$

In this relation s is the mode of the phonon and S is the surface in the reciprocal space on which the phonon energy is constant. The density of states is related with fundamental thermodynamic properties of the system like specific heat capacity c_V and internal energy U. c_V in the low temperature regime is proportional to T^3 and in the high temperature regime it is constant following the Dulong-Petit law($c_V = 3R$).

2.1.1 Born-von Karman model

Historically, the first model describing the lattice dynamics accurately was the Born-von Karman model. It is based on the following assumptions: the system has a discrete translation symmetry, the masses are concentrated in points and the oscillations of the system can be described by a system of harmonic oscillators. For solving this problem it is necessary to make assumptions on the number of neighbouring shells, to get an appropriate description of the lattice dynamics and its choice depends from the final range of the interatomic potential. In the Born-von Karman model it is also possible to introduce additional assumptions about the form of the interaction potential due to symmetry operations. These assumptions significantly reduce the number of free parameters. It also takes into account additional assumptions about the type of interactions. The assumption of axially symmetric forces means that all tangential directions are equivalent. From this assumption with relation(eq. 2.8) interatomic forces could be written in the form:

$$\vec{F} = A\vec{u}_r + B\vec{u}_t, \tag{2.12}$$

where A, B are bond-stretching and bond-bending force constants respectively. In the conventional vector notation equation(eq. 2.12) can be written as:

$$\vec{F} = \frac{A}{r^2}\vec{r}(\vec{r}\cdot\vec{u}) - \frac{B}{r^2}\vec{r}\times(\vec{r}\times\vec{u}) \tag{2.13}$$

in the matrix notation following substitution are used:

$$\vec{r}\cdot\vec{u} = \vec{r}^T\vec{u} \tag{2.14}$$

$$\vec{r}\times\vec{u} = \vec{R}\vec{u} \tag{2.15}$$

Using this formalism from(eq. 2.13, 2.14, 2.15) relations for interatomic forces $\vec{F}$ and force matrix Φ are obtained.

$$\vec{F} = \frac{A}{r^2}\vec{r}\vec{r}^T\vec{u} + \frac{B}{r^2}\vec{R}\vec{R}^T\vec{u} \tag{2.16}$$

$$\Phi = \frac{A}{r^2}\vec{r}\vec{r}^T + \frac{B}{r^2}\vec{R}\vec{R}^T \tag{2.17}$$

This relation can be derived from (eq. 2.3) using the definition of force constants A and B:

$$A = -\frac{\partial^2 \phi}{\partial r^2} \tag{2.18}$$

$$B = -\frac{1}{r}\frac{\partial \phi}{\partial r}. \tag{2.19}$$

Table 2.1: Force matrices for generalised and axially symmetric force matrices respectively.

Atomic position	General			Axially symmetric		
(i 0 0)	$\begin{pmatrix} \alpha_1 & 0 & 0 \\ 0 & \alpha_2 & 0 \\ 0 & 0 & \alpha_2 \end{pmatrix}$			$\begin{pmatrix} A & 0 & 0 \\ 0 & B & 0 \\ 0 & 0 & B \end{pmatrix}$		
(i i 0)	$\begin{pmatrix} \alpha_1 & \beta_1 & 0 \\ \beta_1 & \alpha_1 & 0 \\ 0 & 0 & \alpha_2 \end{pmatrix}$			$\begin{pmatrix} \frac{A+B}{2} & \frac{A-B}{2} & 0 \\ \frac{A-B}{2} & \frac{A+B}{2} & 0 \\ 0 & 0 & B \end{pmatrix}$		
(i i i)	$\begin{pmatrix} \alpha_1 & \beta_1 & \beta_1 \\ \beta_1 & \alpha_1 & \beta_1 \\ \beta_1 & \beta_1 & \alpha_1 \end{pmatrix}$			$\begin{pmatrix} \frac{A+2B}{3} & \frac{A-B}{3} & \frac{A-B}{3} \\ \frac{A-B}{3} & \frac{A+2B}{3} & \frac{A-B}{3} \\ \frac{A-B}{3} & \frac{A-B}{3} & \frac{A+2B}{3} \end{pmatrix}$		
(i j 0)	$\begin{pmatrix} \alpha_1 & \beta_1 & 0 \\ \beta_1 & \alpha_2 & 0 \\ 0 & 0 & \alpha_3 \end{pmatrix}$			$\begin{pmatrix} \frac{Ai^2+Bj^2}{i^2+j^2} & \frac{ij(A-B)}{i^2+j^2} & 0 \\ \frac{ij(A-B)}{i^2+j^2} & \frac{Aj^2+Bi^2}{i^2+j^2} & 0 \\ 0 & 0 & B \end{pmatrix}$		
(i i j)	$\begin{pmatrix} \alpha_1 & \beta_1 & \beta_2 \\ \beta_1 & \alpha_1 & \beta_2 \\ \beta_2 & \beta_2 & \alpha_2 \end{pmatrix}$			$\begin{pmatrix} \frac{Ai^2+B(i^2+j^2)}{2i^2+j^2} & \frac{i^2(A-B)}{2i^2+j^2} & \frac{ij(A-B)}{2i^2+j^2} \\ \frac{i^2(A-B)}{2i^2+j^2} & \frac{Ai^2+B(i^2+j^2)}{2i^2+j^2} & \frac{ij(A-B)}{2i^2+j^2} \\ \frac{ij(A-B)}{2i^2+j^2} & \frac{ij(A-B)}{2i^2+j^2} & \frac{Bi^2+A(i^2+j^2)}{2i^2+j^2} \end{pmatrix}$		
(i j k)	$\begin{pmatrix} \alpha_1 & \beta_1 & \beta_2 \\ \beta_1 & \alpha_2 & \beta_3 \\ \beta_2 & \beta_3 & \alpha_3 \end{pmatrix}$			$\begin{pmatrix} \frac{Ai^2+B(j^2+k^2)}{i^2+j^2+k^2} & \frac{ij(A-B)}{i^2+j^2+k^2} & \frac{ik(A-B)}{i^2+j^2+k^2} \\ \frac{ij(A-B)}{i^2+j^2+k^2} & \frac{Aj^2+B(i^2+k^2)}{i^2+j^2+k^2} & \frac{jk(A-B)}{i^2+j^2+k^2} \\ \frac{ik(A-B)}{i^2+j^2+k^2} & \frac{jk(A-B)}{i^2+j^2+k^2} & \frac{Ak^2+B(i^2+j^2)}{i^2+j^2+k^2} \end{pmatrix}$		

The number of parameters per neighbouring shell for the generalised force matrix is between 2 and 6 and for the axially symmetrical force model it is always 2. This is related to the fact that the generalised force matrices are sensitive to the angular distribution. Knowing the force constant matrices it is straightforward to derive the dynamical matrix. In this thesis, the modelling based on both assumptions: axially symmetrical force constants and generalised force matrices.

From the low-$\vec{q}$ limit it is straightforward to derive the elastic constants, which are a linear combination of the atomic force constants. As an example, the relations between atomic force constants and elastic constants for five neighbouring shells, applying generalised force

matrices, are given:

$$
\begin{aligned}
aC_{11} &= 4\pi^2 m(\alpha_{11} + \alpha_{21} + 4\alpha_{31} + 2\alpha_{32} + 4\alpha_{41} + 9\alpha_{51} + \alpha_{52}), \\
a(C_{12} - C_{44}) &= -2\pi^2 m(2\beta_{11} + 16\beta_{31} + 4\beta_{32} + 8\beta_{41} + 12\beta_{51}), \\
aC_{44} &= 2\pi^2 m(\alpha_{11} + \alpha_{12} + 2\alpha_{22} + 2\alpha_{31} + 10\alpha_{32} + 4\alpha_{41} + 4\alpha_{42} \\
&\quad + \alpha_{51} + 9\alpha_{52} + 10\alpha_{53}).
\end{aligned}
\tag{2.20}
$$

In these formulae α_{ij} and β_{ij} are the diagonal and non-diagonal matrix elements of the generalised force matrix, respectively. i is the number of shells and j is a parameter corresponding to the relative angular difference between points (see table 2.1).

From the dynamical matrix it is possible to calculate $\omega^2(\vec{q})$ in distinct crystallographic directions with high symmetry from a linear combination of the atomic force constants. Thus, the fitting procedure to describe the experimental data is reduced to solving a system of linear equations.

2.1.2   Electron gas contribution

Metal ions are embedded in a sea of electrons which screen the ionic potential of the metal atoms. The model ([Krebs 1965],[Mohammed 1984]) contains the following assumptions: electrons are free fermions at T=0 and the linear response theory is applicable, which leads to the Yukawa potential. It was initially introduced by [Krebs 1965] on bcc alkali metals and later [Mohammed 1984] applied to different fcc transition metals like: Cu, Pt, Au and Ag. In the metal long range interactions due to contributions of the electron gas to the lattice dynamics exist in addition to short range interaction due to screened ionic potential. Interatomic interactions can be explained by superposition of two terms: shell part and ionic part. The shell part corresponds to the Born-von Karman interactions and the ionic part is a screened Coulomb interaction of the metal ions [Krebs 1965].

$$
D_{\alpha\beta}^{TOT} = D_{\alpha\beta}^{BvK} + D_{\alpha\beta}^{e}
\tag{2.21}
$$

Due to the influence of the electron gas, the metal potential is screened, and has the form of a Yukawa-potential[Ashcroft 1976], which is defined by:

$$
V(r) \sim \frac{e^{-k_c r}}{r},
\tag{2.22}
$$

with one free parameter k_c which determines the range of interaction.

$$
D_{\alpha\alpha}^{e} = \frac{1}{4} a^3 k_c^2 k_e \sum_{\vec{h}} \left(\frac{(q_i + h_i)^2}{|\vec{q} + \vec{h}|^2 + (a^2/4\pi^2)k_c^2} - \frac{h_i^2}{h^2 + (a^2/4\pi^2)k_c^2} \right),
\tag{2.23}
$$

$$
D_{\alpha\beta}^{e} = \frac{1}{4} a^3 k_c^2 k_e \sum_{\vec{h}} \left(\frac{(q_i + h_i)(q_j + h_j)}{|\vec{q} + \vec{h}|^2 + (a^2/4\pi^2)k_c^2} - \frac{h_i h_j}{h^2 + (a^2/4\pi^2)k_c^2} \right).
\tag{2.24}
$$

In this model selection rules were included. In the case of a fcc lattice therefore all indices have to be or even or odd. In this model two free parameters k_c and k_e exist. k_e determines the strength and k_c the range of the interaction. From the general properties of an electron gas a value of $k_c=0.6455k_F=0.700$ Å^{-1}[Mohammed 1984] was obtained. k_c was determined using the Thomas-Fermi approximation with an additional correction based on the many-body perturbation theory. To understand the nature of the screening potential better, a starting point is the dielectric function. The solution of the Maxwell equations yields the distribution of the charge which satisfies the Poisson equation [Ashcroft 1976]:

$$-\nabla^2\phi(\vec{r}) = 4\pi\rho(\vec{r}), \tag{2.25}$$

$$-\nabla^2\phi^{ext.}(\vec{r}) = 4\pi\rho^{ext.}(\vec{r}). \tag{2.26}$$

The total density of charge $\rho(\vec{r})$ is a sum of induced and external contributions. In a system with translational symmetry as considered here the dielectric function $\varepsilon(\vec{q})$ and the susceptibility $\chi(\vec{q})$ are defined as:

$$\phi^{ext}(\vec{q}) = \varepsilon(\vec{q})\phi(\vec{q}) \tag{2.27}$$

$$\rho^{ind}(\vec{q}) = \chi(\vec{q})\phi(\vec{q}) \tag{2.28}$$

Using these relations (eq. 2.25, 2.26, 2.27, 2.28) the dielectric function $\varepsilon(\vec{q})$ is obtained:

$$\varepsilon(\vec{q}) = 1 - \frac{4\pi}{q^2}\chi(\vec{q}). \tag{2.29}$$

With the approximation that the potential is a slowly varying function of the distances, the susceptibility is independent of the wave vector $\vec{q}$. From that and the density of states at the Fermi level, the dielectric function is:

$$\varepsilon(\vec{q}) = 1 + \frac{k_{TF}^2}{q^2}. \tag{2.30}$$

For a more accurate description of the electron gas it is necessary to use the approach of the Lindhard function which generelise it. It modifies the range of a screening potential with the factor

$$f(t) = \frac{1}{2} + \frac{1-t^2}{4t}\ln\left|\frac{1+t}{1-t}\right|, \tag{2.31}$$

where are:

$$t_{1,2} = \frac{\pi}{ak_F}(|\vec{q}+\vec{h}|,h). \tag{2.32}$$

and

$$k_F = \sqrt[3]{\frac{9\pi}{4}}\frac{1}{r_s}. \tag{2.33}$$

This term (Eq. 2.21) describes the behaviour of potential in real space in the form:

$$\phi(r) \sim \frac{1}{r^3}\cos(2k_Fr). \tag{2.34}$$

This behaviour is well known as the Friedel oscillation. Including Pauli's exclusion principle leads to the spin-spin correlation function:

$$g(u) = 3\frac{\sin u - u\cos u}{u^3}, \tag{2.35}$$

where are

$$u_{1,2} = \frac{2\pi r_s}{a}(|\vec{q} + \vec{h}|, h). \tag{2.36}$$

Using all these contributions the matrix elements of the dynamical matrix were derived [Mohammed 1984]:

$$D_{\alpha\alpha}^e = \frac{1}{4}a^3 k_c^2 k_e \sum_{\vec{h}} \left(\frac{(q_i + h_i)^2 g^2(u_1)}{|\vec{q} + \vec{h}|^2 + (a^2 k_c^2/4\pi^2)f(t_1)} - \frac{h_i^2 g^2(u_2)}{h^2 + (a^2 k_c^2/4\pi^2)f(t_2)} \right), \tag{2.37}$$

$$D_{\alpha\beta}^e = \frac{1}{4}a^3 k_c^2 k_e \sum_{\vec{h}} \left(\frac{(q_i + h_i)(q_j + h_j) g^2(u_1)}{|\vec{q} + \vec{h}|^2 + (a^2 k_c^2/4\pi^2)f(t_1)} - \frac{h_i h_j g^2(u_2)}{h^2 + (a^2 k_c^2/4\pi^2)f(t_2)} \right), \tag{2.38}$$

with:

$$k_c = 0.353\sqrt{(r_s/a_0)}k_F, \tag{2.39}$$

k_F is the radius of the Fermi sphere, a_0=0.529 Å is the Bohr radius and

$$r_s = \sqrt[3]{3/4\pi n_e} \tag{2.40}$$

is the average interelectronic distance.

In these formulae the discrete translation symmetry of a given crystalline system is taken into account. It is well known that the pure centrally symmetric Born-von Karman model with only centrally symmetric forces will have Cauchy anomaly(C_{12}=C_{44}). This behaviour contradicts the experimental data in most of the systems. It is necessary to add terms without the Cauchy anomaly: taking into account angular dependent forces or adding the electron gas contributions. The present model takes both contributions into account.

2.1.3 Fitting procedure

For the determination of force constants a mean square algorithm is applied, assuming that all experimental points have the same weight:

$$\frac{\partial}{\partial a_{k'}} \sum_j (y_j^c - y_j)^2 = 0 \tag{2.41}$$

where is

$$y_j^c = \sum_k \alpha_{kj} a_k \tag{2.42}$$

and k as the index of the interatomic force constants, a_k as the interatomic force constant and α_{kj} as a coefficient of the form $1 - \cos(\vec{q}\vec{G})$.

Setting

$$X_k = \sum_j y_j \alpha_{kj} \tag{2.43}$$

and

$$A_{kk'} = \sum_j \alpha_{kj} \alpha_{k'j}. \tag{2.44}$$

This system of linear equations may be written in matrix form:

$$X = Aa. \tag{2.45}$$

By solving this system of equations, the interatomic force constants a_k can be obtained. With a higher number of neighbouring shells the system of equations start to be numerically unstable. Therefore different numerical methods for solving the system of linear equations have to be applied. In the applied fitting procedure the Gaussian elimination method was used.

This approach increases the quality of the fit (sum of least squares) with increasing number of neighbouring shells, but the physical meaning of the set of fitted parameters is less defined.

2.2 Elastic theory of continuum

The general theory of elasticity is used for the determination of the relation between cubic system and isotropic system, as well as between elastic constants and moduli.

For investigations on large scale solids, a continuous approximation is valid. From the 1st law of thermodynamics it is necessary to minimize the differential:

$$dU + pdV - TdS \geq 0 \tag{2.46}$$

In solid systems, the volume is nearly independent of temperature and pressure and the corresponding term vanishes: $pdV=0$. The approximation that has to be applied on TdS is not that clear. In a metal where free electrons with characteristic velocity v_F much greater than ultrasound exist, T=const. and the quantity which is minimized is the free energy F. Isolators have an opposite behaviour, so S=const. and the minimisation procedure is applied on the internal energy U only. In the further text the approximation on metallic systems will be written.

When an external force is applied on real systems two types of responses exist: elastic and plastic deformation. When the forces are small enough, the material will return into the initial state before the forces were applied, after external stresses are suppressed, this is known as the elastic regime. In the case of plastic deformation, the situation is opposite and the deformation of the material is permanent. When plastic deformation is applied on

the real system always minor elastic component exists.

The free energy F is a scalar which is invariant to rotations and in the harmonic approximation it can be written in a bilinear form [Ashcroft 1976]:

$$F = F_0 + \frac{1}{2} \int d\vec{r} \sum_{\sigma,\mu,\tau,\nu} \left[\varepsilon_{\sigma\mu} c_{\sigma\mu\tau\nu} \varepsilon_{\tau\nu} \right], \tag{2.47}$$

where $\varepsilon_{\sigma\mu}$ is deformation and $c_{\sigma\mu\tau\nu}$ is tensor of elastic constants which is defined by the relation [Ashcroft 1976]:

$$c_{\sigma\mu\tau\nu} = -\frac{1}{8v} \sum_{\vec{R}} \left[\vec{R}_\sigma D_{\mu\nu} \vec{R}_\tau + \vec{R}_\mu D_{\sigma\nu} \vec{R}_\tau + \vec{R}_\sigma D_{\mu\tau} \vec{R}_\nu + \vec{R}_\mu D_{\sigma\tau} \vec{R}_\nu \right]. \tag{2.48}$$

$c_{\sigma\mu\tau\nu}$ has generally 81 possibilities of different indices. But due to symmetry operations, the number of independent constants is significantly reduced. The number of independent parameters depends on the symmetry of the system. Its number is varied from 21 for triclinic to 3 for a system with cubic symmetry. In the further text the Voigt notation for the tensor of elastic constants in which are 11~1, 22~2, 33~3, 23~4, 13~5 and 12~6 [Brugger 1964] was applied. For investigations on lattice dynamics F_0 is not important and it will be omitted in the further discussion. In this notation [Brugger 1964], the Voigt tensor of elastic constants is equal to [Ashcroft 1976]:

$$\mathbf{C} = \begin{pmatrix} C_{11} & C_{12} & C_{13} & C_{14} & C_{15} & C_{16} \\ C_{12} & C_{22} & C_{23} & C_{24} & C_{25} & C_{26} \\ C_{13} & C_{23} & C_{33} & C_{34} & C_{35} & C_{36} \\ C_{14} & C_{24} & C_{34} & C_{44} & C_{45} & C_{46} \\ C_{15} & C_{25} & C_{35} & C_{45} & C_{55} & C_{56} \\ C_{16} & C_{26} & C_{36} & C_{46} & C_{56} & C_{66} \end{pmatrix}, \tag{2.49}$$

and free energy is equal to:

$$F = (u_{xx}, u_{yy}, u_{zz}, u_{yz}, u_{xz}, u_{xy}) \mathbf{C} (u_{xx}, u_{yy}, u_{zz}, u_{yz}, u_{xz}, u_{xy})^T. \tag{2.50}$$

2.2.1   Elastic theory of an isotropic medium

In the case of isotropic media the Voigt tensor(eq. 2.49, 2.50) is diagonal with the matrix elements equal to: $C_{11}=C_{22}=C_{33}=\lambda$ and $C_{44}=C_{55}=C_{66}=2\mu'$ [Landau 1970].

$$F = \frac{\lambda}{2} \sum_i u_{ii}^2 + \mu' \sum_{ik} u_{ik}^2 \tag{2.51}$$

$$F = 2G \sum_{ikl} (u_{ik}^2 - \frac{1}{3}\delta_{ik} u_{ll}^2) + \frac{B}{2} \sum_l u_{ll}^2, \tag{2.52}$$

where λ and μ' are the Lamé coefficients. The Lamé coefficients are connected to the elastic moduli B and G by:

$$B = \lambda + \frac{2}{3}\mu'. \tag{2.53}$$

$$G = \frac{\mu'}{2}. \tag{2.54}$$

It is straightforward to prove the relation for the free energy F:

$$F = \frac{E}{1+\mu}\left(\sum_{ik} u_{ik}^2 + \frac{\mu}{1-2\mu}\sum_l u_{ll}^2\right), \tag{2.55}$$

where E is the Young modulus and μ the Poisson ratio. This leads to the equation of motion:

$$\rho\frac{d^2\vec{u}}{dt^2} = \frac{E}{1+\mu}\nabla^2\vec{u} + \frac{E}{2(1+\mu)(1-2\mu)}\vec{\nabla}(\vec{\nabla}\vec{u}) \tag{2.56}$$

Therefore, equation (2.56) can be transformed into two wave equations, for longitudinal and transversal polarization, respectively:

$$\frac{d^2 u_{l,t}}{dx^2} = \frac{1}{v_{l,t}^2}\frac{d^2 u_{l,t}}{dt^2}. \tag{2.57}$$

with the velocities of sound for the longitudinal polarization [Landau 1970]:

$$v_l = \sqrt{\frac{E(1-\mu)}{\rho(1+\mu)(1-2\mu)}} = \sqrt{\frac{3B+4G}{3\rho}}. \tag{2.58}$$

and the transversal polarization:

$$v_t = \sqrt{\frac{E}{2\rho(1+\mu)}} = \sqrt{\frac{G}{\rho}}. \tag{2.59}$$

2.2.2   Elastic theory of cubic system

In a system with cubic symmetry the Voigt tensor (eq. 2.49) is reduced to:

$$\mathbf{C} = \begin{pmatrix} C_{11} & C_{12} & C_{12} & & & \\ C_{12} & C_{11} & C_{12} & & 0 & \\ C_{12} & C_{12} & C_{11} & & & \\ & & & C_{44} & 0 & 0 \\ & 0 & & 0 & C_{44} & 0 \\ & & & 0 & 0 & C_4 \end{pmatrix}, \tag{2.60}$$

with three independent elastic constants: C_{11}, C_{12} and C_{44}. They can also be obtained from the gradient of the phonon dispersion curves in high symmetry directions [100], [110]

and [111] in the longwave limit. These gradients are the velocies of sound in different
directions and polarisations.

Table 2.2: Velocities of longitudinal and transversal waves in the cubic system [Willis 1975].

Mod	Direction [100]	Direction [110]	Direction [111]
L	$v_L = \sqrt{\frac{C_{11}}{\rho}}$	$v_L = \sqrt{\frac{C_{11}+C_{12}+2C_{44}}{2\rho}}$	$v_L = \sqrt{\frac{C_{11}+2C_{12}+4C_{44}}{3\rho}}$
T	$v_T = \sqrt{\frac{C_{44}}{\rho}}$	$v_{T_1} = \sqrt{\frac{C_{44}}{\rho}}$	$v_T = \sqrt{\frac{C_{11}-C_{12}+C_{44}}{3\rho}}$
		$v_{T_2} = \sqrt{\frac{C_{11}-C_{12}}{2\rho}}$	

Performing the diagonalisation of the Voigt tensor(eq. 2.49) three different eigenvalues are
obtained. They correspond to cubic symmetry invariants: $C_{11}+2C_{12}$, C_{11}-C_{12} and C_{44}.
These invariants have a well defined physical interpretation: the first one is equal to the
triple bulk modulus(B), and the next two correspond to the resistance of shear deformation
in different directions. They are all positively definit quantities due to the stability of the
system. From these conditions the interval of the ratio C_{12}/C_{11} was obtained, which is
between -0.5 and 1. From the single crystal elastic constants (C_{11}, C_{12} and C_{44}) the
polycrystalline elastic bulk(B) and shear moduli (G) can be derived. In the cubic system
the bulk modulus is given by:

$$B = \frac{C_{11} + 2C_{12}}{3} \tag{2.61}$$

and on the other side the relation between elastic constants and shear modulus is not
uniquely defined and it depends of the method of averaging. Two widely used methods are
the Voigt-Reuss-Hill and Hershey-Kröner-Eshelby averaging method. The shear modulus
G derived from the Hershey-Kröner-Eshelby method is a solution of the following cubic
equation [Ledbetter 1985]:

$$G^3 + \alpha G^2 + \beta G + \gamma = 0, \tag{2.62}$$

where α, β and γ are equal to:

$$\alpha = \frac{5C_{11} + 4C_{12}}{8}, \tag{2.63}$$

$$\beta = -\frac{C_{44}(7C_{11} - 4C_{12})}{8}, \tag{2.64}$$

$$\gamma = -\frac{C_{44}(C_{11} - C_{12})(C_{11} + 2C_{12})}{8}. \tag{2.65}$$

From the Hershey-Kröner-Eshelby method it is straight-forward that $G = G(C_{44}, B, C_{11} - C_{12})$. It is interesting to see that these values also appear in symmetric invariants of the
cubic system. This relation opens the question why the shear modulus is a function of the

bulk modulus. This question presently does not have an appropriate answer. Gairola and Kröner [Gairola 1981] derived the following relation:

$$G = \frac{\alpha_2 G_0^2 + \beta_2 G_0 + \gamma}{G_0^2 + \alpha_1 G_0 + \beta_1}, \tag{2.66}$$

where are:

$$\alpha_1 = \frac{45\varkappa + 24\mu + 36\nu}{40}, \tag{2.67}$$

$$\alpha_2 = \frac{3\mu + 2\nu}{5}, \tag{2.68}$$

$$\beta_1 = \frac{3\varkappa(2\mu + 3\nu)}{20}, \tag{2.69}$$

$$\beta_2 = \frac{3(9\mu\varkappa + 6\nu\varkappa + 20\mu\nu)}{40}, \tag{2.70}$$

$$\varkappa = \frac{C_{11} + 2C_{12}}{3}, \tag{2.71}$$

$$\nu = \frac{C_{11} - C_{12}}{2}, \tag{2.72}$$

$$\mu = C_{44}. \tag{2.73}$$

After solving (eq. 2.66) by using an iterative procedure the obtained result is the same as in the Hershey-Kröner-Eshelby averaging method. Putting the limits $G_0 \longrightarrow \infty$ and $G_0{=}0$ into this equation (eq. 2.66), the Voigt and Reuss results were obtained, respectively. The Voigt-Reuss-Hill averaging method is obtained by the arithmetical middle of: Voigt and Reuss approach. Voigt showed that the shear modulus, derived with the assumption of an uniform elastic strain, G_V is equal to [Voigt 1889]:

$$G_V = \frac{C_{11} - C_{12} + 3C_{44}}{5}. \tag{2.74}$$

Reuss on the other side used the opposite approach, approximation of constant stress [Reuss 1929], and obtained the shear modulus G_R, which is equal to:

$$G_R = 5\left[\frac{4}{C_{11} - C_{12}} + \frac{3}{C_{44}}\right]^{-1}. \tag{2.75}$$

Finally, the shear modulus G_H obtained within Voigt-Reuss-Hill averaging method is equal to:

$$G_H = \frac{G_V + G_R}{2} = \frac{C_{11} - C_{12} + 3C_{44}}{10} + \frac{5}{2}\left[\frac{4}{C_{11} - C_{12}} + \frac{3}{C_{44}}\right]^{-1}. \tag{2.76}$$

Comparing the relations for the shear modulus(eq. 2.74, 2.75) it is seen that the quantity G_V - G_R determines the level of anisotropy in the system. For isotropic systems this leads into the Cauchy relation.

2.2.3   Debye model

The phonon density of states (DOS) g(ω) is generally a non-analytic function of the frequency ω. The DOS of a system which has more than one atom in the basis contains two parts: acoustic and optic. The first models describing the DOS were the Einstein- and the Debye-model. The Einstein model satisfactorily describes the sharp contributions of the optic modes, while the Debye model incorporates the behaviour of the acoustic modes. It is based on the approximation that the frequency is a linear function of the wave number, hence $g(\omega) \sim \omega^2$. The curvature of the obtained parabola fit the low energy part of the DOS. From the fact that the DOS is a finite function on any frequency, the DOS must have a cut-off frequency(ω_D). It is also well known that the Debye frequency is related to the Debye temperature by:

$$\hbar\omega_D = k_B\Theta_D. \tag{2.77}$$

From these relations, together with the Bose-Einstein statistic applicable for phonons, the internal energy is obtained:

$$U = U' - U_0 = \int_0^\infty \frac{g(\omega)\hbar\omega}{e^{\beta\hbar\omega} - 1}d\omega = 3\left(\frac{T}{\Theta_D}\right)^3 \int_0^{\Theta_D/T} \frac{x^3}{e^x - 1}dx. \tag{2.78}$$

$$U_0 = \int_0^\infty g(\omega)\hbar\omega\frac{1}{2}d\omega \tag{2.79}$$

in which β=1/k_BT. From the definition of the heat capacity:

$$C_V = \left(\frac{\partial U}{\partial T}\right)_V = 3\left(\frac{T}{\Theta_D}\right)^3 \int_0^{\Theta_D/T} \frac{x^4 e^x}{(e^x - 1)^2}dx, \tag{2.80}$$

it is seen, that this equation holds for a definition of the Debye temperature, too. Comparing the relations for C_V in the Debye model and in the general case, the following transcendent equation was obtained [Svensson 1967]:

$$\int_0^{\omega_{max}} \frac{(\beta\hbar\omega)^2 e^{\hbar\omega\beta}}{(e^{\beta\hbar\omega} - 1)^2}g(\omega)d\omega = 3\left(\frac{T}{\Theta_D}\right)^3 \int_0^{\Theta_D/T} \frac{x^4 e^x}{(e^x - 1)^2}dx. \tag{2.81}$$

Θ_D(T) is in the low temperature limit equal to the Debye temperature, which is obtained from the low energy part of phonon DOS

$$g(\omega) = \frac{3\varepsilon^2}{(k_B\Theta_D)^3} \tag{2.82}$$

(where ε is the value of the energy transfer).
The Debye temperature can be derived from the elastic properties of polycrystalline solids [Ledbetter 1981]:

$$\Theta_D = \frac{h}{k_B}\left(\frac{4\pi V_a}{3}\right)^{-1/3} v_m. \tag{2.83}$$

Where V_a is the atomic volume and v_m is the velocity of sound averaged over the whole angular range. In isotropic media Debye temperature it is given by [Ledbetter 1981]:

$$\frac{3}{v_m^3} = \frac{1}{v_l^3} + \frac{2}{v_t^3}.$$

(2.84)

Using these relations(eq. 2.83, 2.84) the Einstein-Madelung-Sutherland relation is obtained:

$$\Theta_D = \frac{h}{k_B} \left(\frac{4\pi V}{9N} \right)^{-1/3} \left(\frac{1}{v_l^3} + \frac{2}{v_t^3} \right)^{-1/3}$$

(2.85)

where $G = \rho v_t^2$ and $B = \rho v_l^2 - \frac{4}{3}G$.

2.2.4   Thermal expansion of the crystal

In the real crystalline system, the interatomic potential can be expressed as a sum of harmonic and anharmonic terms. In a system with harmonic forces only, no thermal expansion can occur. Starting from the thermodynamical equations:

$$p = -\left(\frac{\partial F}{\partial V} \right)_T$$

(2.86)

$$T \left(\frac{\partial S}{\partial T} \right)_V = \left(\frac{\partial U}{\partial T} \right)_V,$$

(2.87)

the expression for (eq. 2.86,2.87)leads into an equation for the pressure p:

$$p = -\frac{\partial}{\partial V} \left[U - T \int_0^T \frac{dT'}{T'} \frac{\partial}{\partial T'} U(T', V) \right].$$

(2.88)

Assuming small oscillations around the equilibrium point, the internal energy U can be written in the form [Ashcroft 1976]:

$$U = U_{eq} + \sum_{\vec{k},s} \hbar \omega_s(\vec{k}) \left(n(\omega_s(\vec{k})) + \frac{1}{2} \right),$$

and the pressure p is equal to:

$$p = -\frac{\partial}{\partial V} \left[U_{eq} + \frac{1}{2} \sum_{\vec{k},s} \hbar \omega_s(\vec{k}) \right] + \sum_{\vec{k},s} \left(-\frac{\partial}{\partial V} (\hbar \omega_s(\vec{k})) \right) \times n(\omega_s(\vec{k})).$$

(2.89)

Starting from the definition of the linear expansion coefficient α in the approximation of isotropic expansion we get:

$$\alpha = \frac{1}{l} \left(\frac{\partial l}{\partial T} \right)_p = \frac{1}{3B} \left(\frac{\partial p}{\partial T} \right)_V.$$

(2.90)

The Grüneisen parameter $\gamma_{\vec{k},s}$ for a given mode [Ashcroft 1976] is defined:

$$\gamma_{\vec{k},s} = \frac{V}{\omega_s(\vec{k})} \frac{\partial \omega_s(\vec{k})}{\partial V}.$$ (2.91)

Using the equation (eq. 2.89, 2.90, 2.91) the correlation between the linear expansion coefficient and the total Grüneisen parameter γ can be obtained.

$$\alpha = \frac{\gamma c_v}{3B}.$$ (2.92)

The dependence of the Grüneisen parameter from temperature is very weak and almost the whole dependency can be included in the specific heat capacity. In metals also the contributions from the electron gas to the heat capacity should be taken into account. But this contribution is important only at very low temperatures, i.e. in the 10 K region. In all other temperature ranges the contribution from the electron gas is too small and can be neglected.

Chapter 3

Experimental methods

In this part of the thesis the experimental methods which were applied on the austenitic stainless steels, hydrogenated austenitic stainless steels and copper selenide systems were introduced. For the structure determination powder diffraction was used (laboratory X-ray, synchrotron and neutron diffraction). For the investigation of lattice dynamics inelastic neutron scattering(INS) was applied on single crystals as well as on polycrystalline samples.

3.1 Diffraction

The diffraction method is an adequate technique for structural investigations. In the case of atoms building a perfect crystal lattice, also well defined crystal planes exist. Scattering on them is described by the well known Bragg law. It is straightforward to see, that in the case of constructive interference maximum points of intensity are defined by the relation:

$$\vec{k}_i - \vec{k}_f = \vec{\tau} \tag{3.1}$$

where $\vec{\tau}$ is the vector of reciprocal lattice which leads to the Bragg law:

$$n\lambda = 2d\sin\theta. \tag{3.2}$$

To obtain realistic physical information from the diffraction studies it is necessary to introduce the concept of the "real crystal" instead of an ideal one. The first step is to exchange an atom as a point scatterer by its spacial distribution of charge($\rho(\vec{r})$) which gives the atomic form factor $F(\vec{Q})$:

$$F(\vec{Q}) = \int_{cell} \rho(\vec{r})e^{i\vec{Q}\vec{r}}dV. \tag{3.3}$$

Where are $\vec{Q}$ is value of transfer of momentum:

$$\vec{Q} = \vec{k}_i - \vec{k}_f. \tag{3.4}$$

This is the relation for the structure factor $F(\vec{Q})$ and can be presented as a linear combination of atomic charge densities($f_k(\vec{Q})$) in the form:

$$F(\vec{Q}) = \sum_{k=1}^{n} f_k(\vec{Q})e^{2\pi i \vec{K}\vec{r}(\kappa)}, \tag{3.5}$$

which is in the case of neutrons described by the equivalent relation:

$$F(\vec{Q}) = \sum_{k=1}^{n} b_k e^{2\pi i \vec{K}\vec{r}(\kappa)}, \tag{3.6}$$

where b_k is the scattering length. For crystalline system relation for form factors:

$$F_{hkl} = \sum_{j=1}^{n} b_j T_j e^{2\pi i(hx_j + ky_j + lz_j)}. \tag{3.7}$$

The total intensity of a reflection in powder diffraction is equal to [Willis 1975]:

$$E_{hkl} \sim \frac{1 + \cos^2(\theta)}{2\sin^2(2\theta)} |F_{hkl}|^2. \tag{3.8}$$

It contains two important parameters: p polarization factor which is equal to:

$$p = \frac{1}{2}\big(1 + \cos^2(\theta)\big), \tag{3.9}$$

for X-rays and in the case of non-polarised neutrons it is equal to $p = 1$.

$$L = 1/\sin(2\theta) \tag{3.10}$$

is the Lorentz factor which is described by the geometry of the experiment. If thermal vibration is taken into account, the form factors are transformed into:

$$F = \sum_{k=1}^{n} f_k e^{2\pi i \vec{K}(\vec{r}_k + \vec{\delta}_k)}, \tag{3.11}$$

$$|F|^2 = \sum_{k=1,k'=1}^{n} f_k f_{k'}^* e^{2\pi i \vec{K}(\vec{r}_k - \vec{r}_{k'})} \left\langle e^{2\pi i \vec{K}(\vec{\delta}_k - \vec{\delta}_{k'})} \right\rangle. \tag{3.12}$$

Using the relation for the mean value of displacement of harmonic crystall in thermal equilibrium it is equal to:

$$< e^{ix} > = e^{-\frac{1}{2}<x^2>}, \tag{3.13}$$

which leads to a correction of the form factor F due to the influence of the temperature [Willis 1975],

$$F = \sum_{k=1}^{n} f_k e^{-M_k} e^{2\pi i \vec{K}\vec{r}_k} \qquad or \qquad f_T = f_0 e^{-M}. \tag{3.14}$$

M is defined by:

$$M = 8\pi^2 < \delta^2 > \left(\frac{\sin\theta}{\lambda}\right)^2 = B_{iso}\left(\frac{\sin\theta}{\lambda}\right)^2. \tag{3.15}$$

In this formula the parameter for isotropic thermal displacement is defined as $B_{iso} = 8\pi^2 < \delta^2 >$. For an anisotropic system, B_{iso} becomes a symmetrical tensor of second rang, and therefore have up to 3 independent components. The number of independent parameters depends only on the symmetry of the given system. Increasing the value of the parameter for thermal displacement the intensity in the Bragg peaks is decreased and, simultaneously, the contribution of diffuse scattering to the pattern is increased. The decrease in intensity in the Bragg peaks is much more pronounced at higher diffraction angles θ.

The mean square atomic displacement can also be connected to thermal properties of the system in the thermodynamical equilibrium.

In the case of small oscillations around the equilibrium point they are well described by a harmonic oscillator:

$$H = \frac{p^2}{2m} + \frac{m\omega^2 x^2}{2}, \tag{3.16}$$

with the eigenvalues (energies):

$$E = \hbar\omega(n + \frac{1}{2}). \tag{3.17}$$

From this relation the mean squared displacement $< (\Delta x)^2 >$ is obtained:

$$< (\Delta x)^2 >= \frac{\hbar^2}{2m} \int_0^\infty \frac{g(\omega)}{\omega} \frac{e^{\beta\hbar\omega} + 1}{e^{\beta\hbar\omega} - 1} d\omega. \tag{3.18}$$

In the given equation (eq. 3.18) the parameter β is defined as $\beta = 1/k_B T$. When the Debye model is valid, this equation 3.18 transforms into [Willis 1975]:

$$< (\Delta x)^2 >= \frac{3\hbar^2 T}{mk_B\Theta_D}\left(\Phi(\Theta_D/T) + \frac{\Theta_D}{4T}\right), \tag{3.19}$$

where $\Phi(x)$ is defined by:

$$\Phi(x) = \frac{1}{x} \int_0^x \frac{y\,dy}{e^y - 1}. \tag{3.20}$$

In the low temperature region the mean square displacement is almost constant:

$$< (\Delta x)^2 >= \frac{3\hbar^2}{4mk_B\Theta_D}, \tag{3.21}$$

and whereas in the high temperature region $< (\Delta x)^2 >$ starts to grow linearly with increasing temperature:

$$< (\Delta x)^2 >= \frac{3\hbar^2 T}{mk_B\Theta_D^2}. \tag{3.22}$$

The diffraction experiments were performed either with X-rays or neutrons. Neutron diffraction is characterised by a relatively low energy resolution ($\Delta\varepsilon/\varepsilon$), but on the other

hand it is possible to investigate magnetic structures due to their interaction with the magnetic moments of the neutron. Because of the higher differential cross section compared to X-rays it is possible to observe light elements like hydrogen, which are almost non-observable by X-rays. In the case of X-ray diffraction, the interaction of the radiation takes place with the electrons, and therefore the differential cross section increases with the number of electrons. A special type of X-ray diffraction is that with synchrotron radiation. It is almost linearly polarised and because of this property it is an appropriate method for the investigation of magnetism. An additional advantage of synchrotron radiation compared to conventional X-ray tube radiation is a much higher intensity and energy resolution.

3.2 Inelastic neutron scattering

For measuring the phonon dispersion curves X-rays as well as neutrons can be used as a probe. The X-ray method can be applied only in the very low energy part of the dispersion curves, whereas INS is the only method applicable to all regions of the phonon spectra. A criterion to choose the probe is a transfer of energy and momentum as close as possible to the phonons which are investigated. An additional difference is the penetration depth, which is a few orders of magnitude higher for neutrons than for X-rays. Due to that, neutrons are especially appropriate to bulk materials.

Intensity I of scattered neutrons is:

$$I \sim \frac{d^2\sigma}{d\omega d\Omega}. \tag{3.23}$$

According to the Fermi golden rule the double differential cross section of scattering particles $d^2\sigma/d\omega d\Omega$ is equal to [Kittel 1963]:

$$\frac{d^2\sigma}{d\omega d\Omega} = \frac{k'}{k}\left(\frac{m}{2\pi}\right)^2 | < k'f|H'|ki > |^2 \delta(\omega - \omega_i + \omega_f). \tag{3.24}$$

The interaction of neutrons with matter is weak, so the Born approximation describes the scattering process well. The initial and final state of the scattered neutron can be described as a plane wave of form $e^{i\vec{k}\vec{x}}$. In this case, the matrix element of the transition matrix is equal to:

$$< k'f|H'|ki > = V_{\vec{k}}\sum_j < f|e^{i\vec{k}\vec{x}_j}|i >, \tag{3.25}$$

where $V_{\vec{k}}$ is the Fourier transform of the interaction potential. From this the double differential cross section is equal to:

$$\frac{d^2\sigma}{d\omega d\Omega} = \frac{k'}{k}\left(\frac{m}{2\pi}\right)^2 |V_{\vec{k}}|^2 \frac{1}{2\pi}\int_{-\infty}^{\infty} dt e^{-i\omega t}\sum_{jl} < e^{-i\vec{k}\vec{x}_j(0)} e^{i\vec{k}\vec{x}_l(t)} >_T . \tag{3.26}$$

Where $< ... >_T$ is averaged over all possible states at the final thermodynamical temperature T. It is convenient to factorise the double differential cross section in the form:

$$\frac{d^2\sigma}{d\omega d\Omega} = A_{\vec{k}} S(\vec{k}, \omega), \tag{3.27}$$

with:

$$A_{\vec{k}} = \frac{k'}{k} \left(\frac{m}{2\pi}\right)^2 |V_{\vec{k}}|^2 \tag{3.28}$$

and scattering function $S(\vec{k}, \omega)$:

$$S(\vec{k}, \omega) = \frac{1}{2\pi} \int_{-\infty}^{\infty} dt e^{-i\omega t} \sum_{jl} < e^{-i\vec{k}\vec{x}_j(0)} e^{i\vec{k}\vec{x}_l(t)} >_T . \tag{3.29}$$

One of the standard models for the description of the interaction between the neutron and the nucleus is the Fermi pseudopotential $V(r) = (2\pi)/mb_i\delta(\vec{r} - \vec{R}_i)$. b_i is the scattering length and its sign describes whether the force between them is attractive or repulsive [Ashcroft 1976](positive sign of b_i is given for attractive and negative sign of b_i is given for repulsive potential).

$$\frac{d\sigma}{d\Omega} = \underbrace{| < b^2 > | \left| \sum_l e^{i\vec{k}\vec{x}_l} \right|}_{coherent} + \underbrace{N(< |b|^2| - | < b > |^2)}_{incoherent} \tag{3.30}$$

The scattering length for coherent scattering is equal to:

$$b_i^{coh} = < b_i > \tag{3.31}$$

and for incoherent scattering it is:

$$b_i^{inc} = \sqrt{< b_i^2 > - < b_i >^2}. \tag{3.32}$$

Incoherent scattering is isotropic, and can be caused by different isotopes (e.g. different Ni isotopes) or due to the spin (H). The nature of incoherent scattering is due to nucleon-nucleon interaction which also had some spin component. For most of the isotopes coherent scattering is much stronger than incoherent, but some exceptions exist. In the case of light elements with few nuclei due to great difference in strength of interaction with parallel and antiparallel oriented spins, this behaviour is especially pronounced in the case of hydrogen. This is extremely important in the investigation of hydrogen-metal systems.

When neutron beam hit in matter two kind of processes could occur: neutron pass through the sample without interaction and part interact with matter. The interaction between neutrons and matter can either be elastic or inelastic. An elastic process is described by a change in direction of the momentum of the scattered beam without changing its energy.

In this case only information about the structure and none about the lattice dynamics can be obtained. An inelastic process can be described by

$$\vec{p'} - \vec{p} = \vec{K} \tag{3.33}$$

where $\vec{p}$ is the momentum of incident neutron, $\vec{p'}$ that of the scattered neutron and $\vec{K}$ a vector of the reciprocal lattice. In inelastic neutron scattering single or multiple phonon processes can occur. In the case of single phonon processes the phonon is absorbed or emitted which is given by the relation:

$$\frac{p^2}{2m_n} - \frac{p'^2}{2m_n} = \pm \hbar \omega (\vec{p} - \vec{p'}), \tag{3.34}$$

in which the "plus"-sign is for the phonon emission and "minus" is for an absorption process. When a two-phonon process occurs the conservation laws lead to a much more complicated relation:

$$\frac{p^2}{2m_n} - \frac{p'^2}{2m_n} = \pm \hbar \omega (\vec{p} - \vec{k} - \vec{p'}) \pm \hbar \omega (\vec{k}). \tag{3.35}$$

Whereas in the single phonon process it is possible to find a unique solution for the equation 3.35 this no longer holds for a double or multiple phonon process. Due to that the input energy of the neutron is chosen in such a way that multiple phonon processes are much less probable. In the case of acoustic phonons it is about 10-20 meV corresponding to a wavelength of 1-1.5 Å.

A primary source for neutrons are either fission reactors or spallation sources. In the case of the neutron fission isotope used is U-235. When the nucleus of uranium is hit by slow neutrons it goes in excited state U-236 which decays in fragments, e.g. Kr-92, Ba-141 and 3 neutrons which start a chain reaction. The energy of these neutrons is rather low and ranges from few MeV to few meV by moderator, which is the interesting range for the investigation of solids. Another source for neutrons are spallation sources, where high energetic protons with energies of 1-2 GeV hit a target of heavy nuclei like lead. The nuclei will go in a highly excited state and a cascade of neutrons will be generated. Spallation sources are characterised by a much higher number of neutrons per input neutron. Second important difference between spallation source and nuclear reactor is that spallation source work in pulse mode and nuclear reactor mainly in continuous mode.
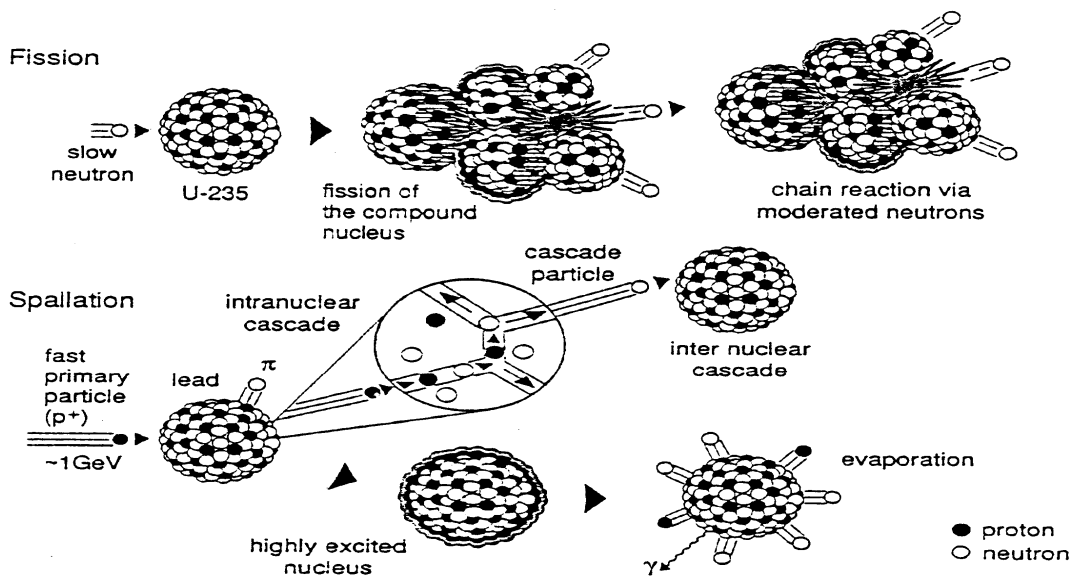
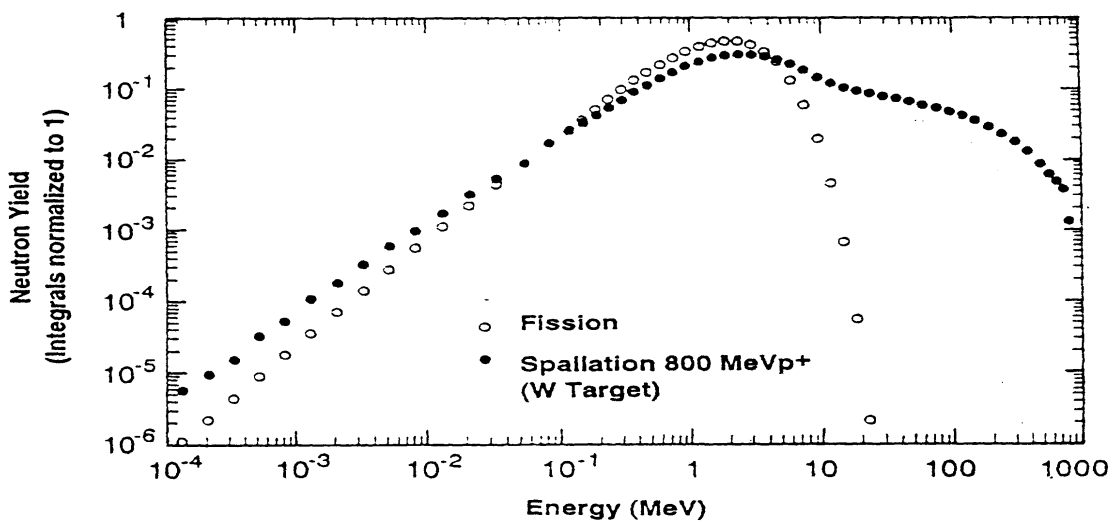Figure 3.1: Schematic representation of fission and spallation[Kádár 1999].

Figure 3.2: Intensity of the created neutrons for different sources[Kádár 1999].

Table 3.1: Energy range for neutrons.

	Source	Energy [eV]	Wavelength[Å]	Application
Epithermal	Spallation 2% of reactor	≤ 0.3	<0.5	Exitation in metals
Hot	Graphite 2000 C	0.3-0.08	0.5-1.0	Structure and dynamics
Thermal	moderation D_2O	0.1-0.02	0.8-2.0	
Cold	moderation H_2	0.02-0.002	2.0-20.0	Slow molecular motion Small angle scattering
Ultra Cold	Turbine	$0.002\text{-}10^{-6}$	20.0-100.0	Large molecules

These neutrons are slowed down by a suitable moderator. As moderator materials usually light elements are used, especially heavy water or graphite.

3.2.1   Basic concept of the time of flight method

Thermal neutrons from reactors have velocities in the order of some km/s, so their moments and energies can be well defined by a flight path of a few meters. The quantity measured in an inelastic neutron experiment is the energy transfer. The measurement can be performed in two modes: with a fixed incident energy of the beam by monochromator and the final energy of the scattered beam measured; or vice-versa. This defines two sorts of time of flight (TOF) [Kádár 1999] spectrometers, one with a direct geometry selecting the energy of the incident beam or an indirect geometry with an energy selection in the scattered beam. Energy selection can be performed by a chopper wheel or by reflection on a single crystal monochromator. From the equations of conservation the regions of space $(\vec{Q}, \omega)$ possible to measure are defined. In the direct method the relation which defines the allowed region of $(\vec{Q}, \omega)$ is given by [Kádár 1999]:

$$\frac{\hbar^2 \vec{Q}^2}{2m_n} = 2\varepsilon_i - \hbar\omega - 2\cos\theta\sqrt{\varepsilon_i(\varepsilon_i - \hbar\omega)} \tag{3.36}$$

and for the indirect method the allowed region is

$$\frac{\hbar^2 \vec{Q}^2}{2m_n} = 2\varepsilon_f + \hbar\omega - 2\cos\theta\sqrt{\varepsilon_f(\varepsilon_f + \hbar\omega)}. \tag{3.37}$$

Where θ is the angle between the incident and scattered momentum vector. When the direct geometry is used the incident energy is monochromated by reflection on a single crystal or by use of a chopper wheel. The chopper consists of a metal plate rotating with a high angular velocity. The plate is made from a durable light material, e.g. aluminium, which is capable to resist the high centrifugal forces from the rotation. It is also important that the material is transparent to neutrons. Most of the surface is covered by a material

with a high absorption coefficient for neutrons like gadolinium or boron. On the surface
"window" exist which allows passing of neutrons. With a single chopper it is possible to
choose neutrons with energy interval, with several choppers it is possible to create pulses of
neutrons with a well defined energy. For energy determination of the incident neutrons at
least two choppers are necessary. Behind the sample an energy dispersive detector system is
located, which measures energy and momentum of the scattered neutron beam. A general
property of all TOF spectrometers is the simultaneous coverage of the Q-ω space together
with a broad energy range between meV and 100 eV. Energy of neutrons is only determined
with frequency and distances between choppers. Therefore it is possible to cover a broad
scale of energy range with TOF spectrometers.

Experiments can also be performed in two modes, investigation of energy gain and energy
loss mode. Starting from relations 3.23 and 3.26 the relation for dynamical structure factor
$S(\vec{Q}, \omega)$ is obtained:

$$S(\vec{Q}, \omega) \sim \frac{1}{\omega} \begin{cases} \frac{Q^2 e^{-<u^2>Q^2}}{n(\omega)+1} g(\omega) & \text{energy loss process} \\ \frac{Q^2 e^{-<u^2>Q^2}}{n(\omega)} g(\omega) & \text{energy gain process.} \end{cases} \tag{3.38}$$

From relation 3.38 it straightforward to conclude that intensity in energy loss spectroscopy
is much higher and almost independent of temperature.

In terms of lattice dynamics the TOF method is usually used for the determination of the
phonon density of states. To separate contributions from sample and container, the empty
container is measured independently and therefore its contribution can be separated from
the total signal.

Multiphonon correction

The measured intensity after background subtraction in inelastic neutron scattering can
be described by three contributions: an elastic term, single phonon and multiphonon in-
elastic processes. For investigation of the lattice dynamics only the single phonon pro-
cesses are interesting, so it is necessary to remove the multiphonon contribution to the
signal. Its contribution is explained by the relations([Sjölander 1958], [Dawidowski 1998]
and [Dawidowski 2002]):

$$S(Q, \omega) = e^{-\alpha Q^2} \delta(\omega) + \sum_{n=1}^{\infty} \frac{1}{n!} e^{-\alpha Q^2} (\alpha Q^2)^n U_n(\omega). \tag{3.39}$$

Where α is related to the Debye-Waller exponent $(2W)$ by the relation:

$$\alpha = \frac{2W}{Q^2} = \frac{<u^2>}{3} = \frac{\hbar^2}{2m} \int_0^\infty \frac{g(\omega)}{\omega} (2n(\omega) + 1) d\omega. \tag{3.40}$$

In this relation n(ω) is the Bose-Einstein distribution and m is the average mass of the
scattering atoms. U$_n$ is defined by:

$$U_1(\omega) = \frac{\hbar^2}{2m\alpha} \frac{g(\omega)}{\omega} (n(\omega) + 1), \tag{3.41}$$

and

$$U_n(\omega) = \int_{-\infty}^{\infty} U_{n-1}(\omega')U_1(\omega - \omega')d\omega'. \tag{3.42}$$

For a starting assumption in the iteration procedure only the first term of expansion is used relation (3.39),

$$g(\omega) \approx \frac{\omega S_{exp}(Q,\omega)}{Q^2 e^{-\alpha Q^2}(n(\omega)+1)}. \tag{3.43}$$

From this relation for density of states(eq. 3.41) $U_1^{(0)}$ is calculated, which is a starting point of the iteration. From $U_1^{(0)}$(eq. 3.42) is the $U_m^{(0)}$ is obtained which is the first correction of the multiphonon part. This correction is equal to the sum of the $U_n^{(0)}$ where n determines how many terms in the expansion are taken into account. The first correction in the function $U_1^{(0)}$ is given by:

$$U_1^{(1)} = \frac{U_1^{(0)}(\omega)}{1 + \frac{U_m^{(0)}(\omega)}{U_1^{(0)}(\omega)}}, \tag{3.44}$$

and the final correction therefore is,

$$U_1^{(n)} = \frac{U_1^{(0)}(\omega)}{1 + \frac{U_m^{(n-1)}(\omega)}{U_1^{(n-1)}(\omega)}}. \tag{3.45}$$

The number of iterations strongly depends on the factor α but usually converges rapidly, after a few iterations only. From the $U_1^{(n)}$ the corrected density of states is obtained.

3.2.2   Basic concept of the Triple-Axis Spectrometer

The selection of the $\vec{k}_i(\vec{k}_f)$ is determined by Bragg scattering at the monochromator and the analyser. Each configuration of the spectrometer leads to a well defined point in the $(\vec{Q},\omega)$ space [Kádár 1999]. From the conservation laws further relations are obtained:

$$\text{momentum conservation} \quad \vec{k}_i - \vec{k}_f = \vec{Q} = \vec{\tau} \pm \vec{q}, \tag{3.46}$$

and

$$\text{energy conservation} \quad \frac{\hbar^2 \vec{k}_i^2}{2m_n} - \frac{\hbar^2 \vec{k}_f^2}{2m_n} = \hbar\omega. \tag{3.47}$$

Where $\vec{Q}$ is the transfer of momentum, $\vec{\tau}$ the vector of the reciprocal lattice and $\vec{q}$ is the phonon wave vector in the first Brillouin zone. This method is usually performed on a single-crystalline sample. Triple-axis spectrometer (TAS) experiments can be performed in two modes: constant energy and constant momentum transfer. In this thesis, the experiments are performed in constant Q mode. The intensity of the neutron beam is measured around a given point of the reciprocal space as function of a energy. From comparison of the triple-axis spectrometer (TAS) and the TOF method it is seen that the

TOF method has the advantage of a faster and more efficient data collection and this is most important for polycrystalline samples. In the case of single crystalline samples it is nontrivial to obtain data from the TOF data because orientation is important and most of the data are collected in non-symmetrical direction. In this case a triple-axis spectrometer is a much better choice for the investigation of the phonon dispersion curves in a single crystal.

3.3 Hydrogenation of austenitic stainless steels

To incorporate hydrogen into austenitic stainless steels two experimental techniques can be used: electrolytic charging and loading with high pressure cells.

In the case of cathodic charging hydrogen penetrates the sample in a very thin layer only, which leads to a non-homogenous distribution of hydrogen and a significant internal stress occurs. With cathodic charging additional problems exist in neutron investigation. The mean free path of neutron is much longer than the penetration depth of hydrogen in matter, so the hydrogen influence is almost invisible to neutrons.

For all these reasons hydrogenation of austenitic stainless steels was performed by high pressure. It functions in the way that samples were stored in the cell which contains kaolin wool and mica. As source of hydrogen AlH_3 was used. This system was heated up to 250 °C. At this temperature AlH_3 decays which provide hydrogen for the loadings. Pressure was applied on this cell (fig. 3.3)
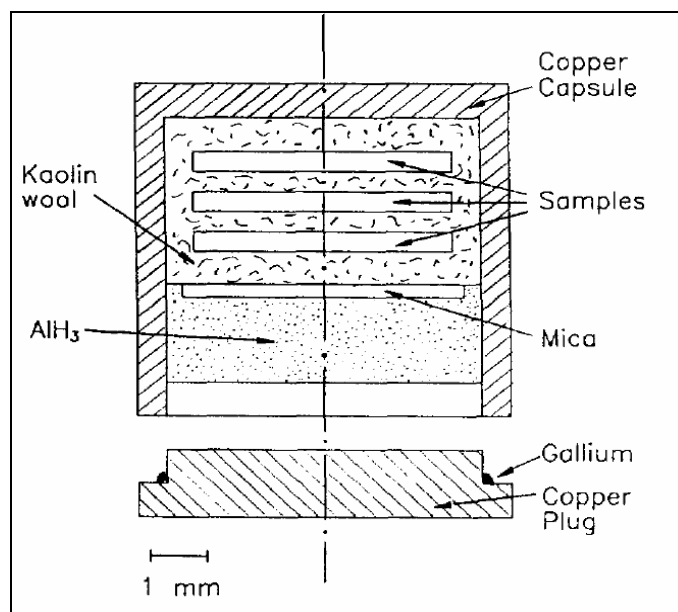

Figure 3.3: High pressure cell in Chernogolovka [Antonov 1996].

To my best knowledge this study is the first neutron scattering study on hydrogen charged samples by a high-pressure cell.

Chapter 4

Lattice dynamics of austenitic stainless steels

4.1   Diffraction study

Diffraction studies are necessary for investigation of lattice dynamics. Diffraction experiments on polycrystalline samples[1] were performed on a Siemens D500 (diffractometer) with CuK_α radiation. In both austenitic stainless steels: Fe-18Cr-16Ni-10Mn and Fe-18Cr-12Ni-2Mo the lattice parameter was estimated to a=3.593 Å. Diffraction data analysis also shows, that Fe-18Cr-16Ni-10Mn and Fe-18Cr-12Ni-2Mo only contain the γ-phase.
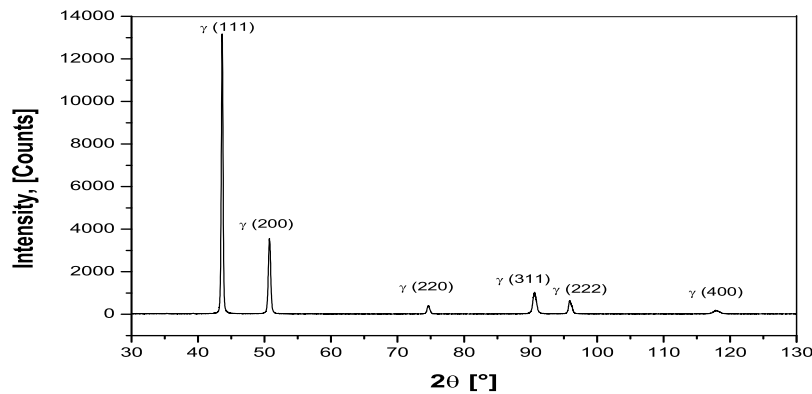

Figure 4.1: X-ray powder diffraction pattern from Fe-18Cr-16Ni-10Mn

The results of the diffraction studies were used in the INS measurements as well as a base for modelling of lattice dynamics.

---

[1]experiments were performed by Markus Hölzel

4.2   Phonon dispersion curves

For the investigation of the lattice dynamics inelastic neutron scattering on single crystals and polycrystalline samples were used. From single crystals of austenitic stainless steels it is possible to determine the phonon dispersive curves.

4.2.1   Experiment

Single crystals of $15\times15\times25$ mm^3 (Fe-18Cr-12Ni-2Mo) and $8\times8\times40$ mm^3 (Fe-18Cr-16Ni-10Mn) have been prepared by the Bridgman method at the Tomsk State University, Russia. The measurements[2] of the dispersion branches have been carried out at the triple-axis spectrometer UNIDAS at *Forschungszentrum Jülich*, Germany. Both steels have fcc structure with space group Fm$\bar{3}$m with a corresponding lattice parameter of 3.593 Å , obtained from X-ray diffraction data (fig. 4.1). The mosaic spread of Fe-18Cr-12Ni-2Mo was determined to 40$'$, whereas in the case of Fe-18Cr-16Ni-10Mn a mosaic spread of 30$'$ was found. All measurements of both steels have been carried out in constant-Q mode with a fixed incident neutron energy of 14.74 meV. Alignments of the crystal were chosen to have the (110) plane and (001) plane coinciding with the scattering plane. Measurements of equivalent points in different Brillouin zones and different alignments were performed to optimize the focussing conditions and to distinguish between the different polarizations of the phonons. After that, from a scan containing intensity versus energy at a given wave vector and polarization the value of the energy and the corresponding error bars were obtained by fitting a Gaussian peak profile.

4.2.2   Results

Experimental data were analysed in the frame of the Born-von Karman model. The dispersion branches of austenitic stainless steels Fe-18Cr-12Ni-2Mo and Fe-18Cr-16Ni-10Mn(Fig. 4.2) are similar to those of various other fcc systems, for instance Ca [Stassis 1983], Yb [Stassis 1982], γ-Fe and Fe$_{0.7}$Ni$_{0.3}$ [Hallman 1969]. Their high similarity is supposedly related to the similar lattice parameters and densities.
Fe-18Cr-12Ni-2Mo shows a slightly concave curvature for the T$_1$-[110] direction in the low q region. A similar behaviour was also observed in Ca[Stassis 1983], Yb[Stassis 1982], γ-Fe[Zarestky 1987] and Fe$_{0.7}$Ni$_{0.3}$ [Hallman 1969]. This behaviour is, however, not observed in the Fe-18Cr-16Ni-10Mn. One possible reason for the behaviour in the (fig. 4.2) could be an anharmonicity of the potential. Anharmonicity results in a different damping of the longitudinal and transversal modes of vibration. Additionally, electron-phonon interaction could result in such a concave curvature [Stassis 1983, Stassis 1982].
Significant differences between Fe-18Cr-12Ni-2Mo and Fe-18Cr-16Ni-10Mn can be found in the L-[110] branch, where Fe-18Cr-12Ni-2Mo shows lower frequencies.

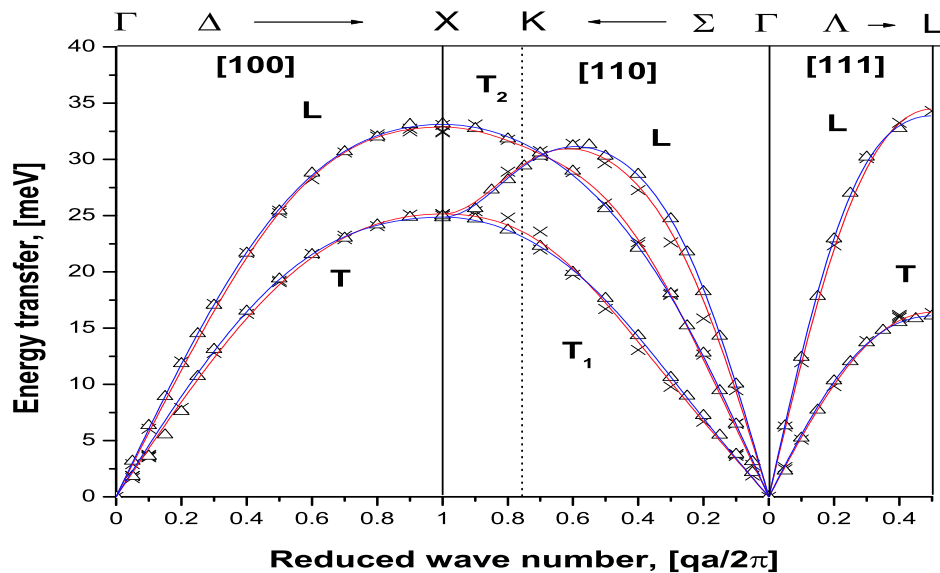[2]experiments were performed by Markus Hölzel

Figure 4.2: Measured phonon dispersion curves for Fe-18Cr-12Ni-2Mo ($\times$), Fe-18Cr-16Ni-10Mn ($\triangle$), calculations based on the Born-von Karman model, 5 neighbouring shells, generalized force matrix, for Fe-18Cr-12Ni-2Mo (—) and Fe-18Cr-16Ni-10Mn (—).
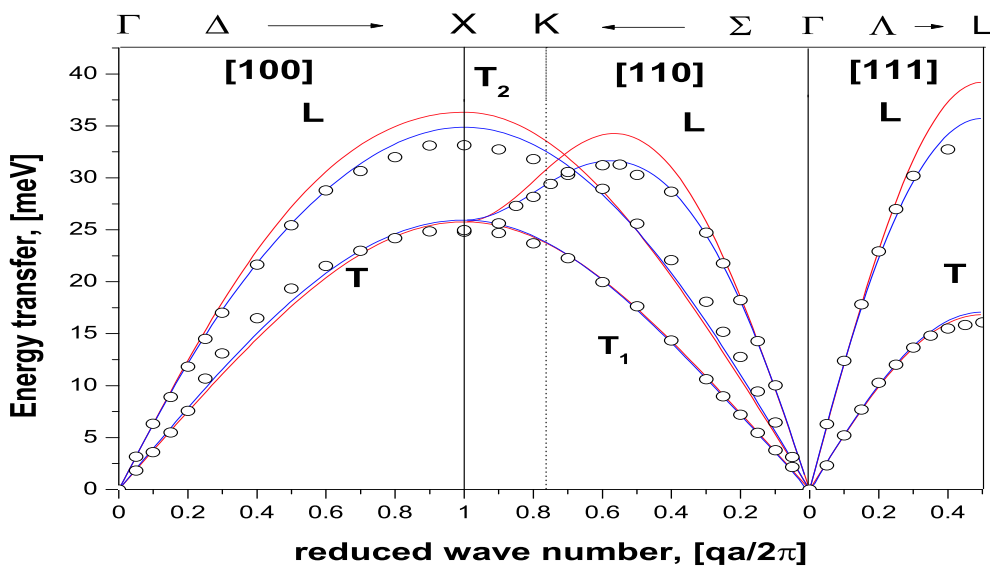

Figure 4.3: Measured phonon dispersion curve for Fe-18Cr-16Ni-10Mn ($\circ$), calculations based on the Born-von Karman model, 2 neighbouring shells, generalized force matrix without (—) and with electron gas contributions (—).

Data were analysed by model calculations based on the Born-von Karman interactions using the generalised force matrices as well as the approximation of axially symmetrical interactions. The model calculations were carried out up to the eighth nearest-neighbour shell using the generalised and axially symmetric force matrix model. In the next model a reduced number of shells was used(free parameters), but an additional term was added to the dynamical matrix. This term simulates contributions from the electron gas. The electronic term in the dynamical matrix introduces only one refinable parameter(eq. 2.37, 2.38), k_e=18-20 GPa, the bulk modulus of the electron gas [Mohammed 1984]. From the general properties of the electron gas a value of k_c=0.6455k_F=0.700 Å^{-1} was obtained. k_c was determined using the Thomas-Fermi approximation with an additional correction based on the many-body perturbation theory.

From (fig. 4.2) it can be seen that for second nearest-neighbour shell with contributions from the electron gas leads to a significant improvement of the description of the experimental data compared to the conventional Born-von Karman model. Because of the long range Coulomb forces only a few neighbouring shells are required for an adequate fit to the experimental points. The improvement is especially pronounced in the regions close to the edges of the Brillouin zone in all directions. This effect is probably related to the screening of the Coulomb potential due to the presence of conduction electrons.

Table 4.1: Elastic properties of austenitic stainless steels: Fe-18Cr-12Ni-2Mo and Fe-18Cr-16Ni-10Mn obtained from the phonon dispersion curves and compared with ultrasonic studies.

	Fe-18Cr-12Ni-2Mo			Fe-18Cr-16Ni-10Mn		
	BvK	low q	Ultrasonic	BvK	low q	Ultrasonic
	5 neigh.	fitting	[Ledbetter 1981]	5 neigh.	fitting	[Kim 1994]
C_{11}[GPa]	195.7	195.3	206	221.8	199.4	206.8
C_{12}[GPa]	130.1	132.1	133	154.0	125.3	134.6
C_{44}[GPa]	111.0	107.9	119	125.4	101.6	114.7
G [GPa]	68.3	67.2	74.2	74.5	68.5	72.3
B [GPa]	152.0	153.2	157.3	176.6	150.0	158.7
E [GPa]	180.4	175.8	194.7	199.0	178.5	190.4
ν	0.30	0.31	0.29	0.31	0.30	0.30
C_{12}/C_{11}	0.665	0.676	0.647	0.694	0.628	0.651
A	3.38	3.41	3.27	3.70	2.74	3.18

The Zener anisotropy A is defined as:

$$A = \frac{2C_{44}}{C_{11} - C_{12}}. \tag{4.1}$$

For the Fe-18Cr-12Ni-2Mo and Fe-18Cr-16Ni-10Mn the result based on Born-von Karman model with generalised force matrix is presented in table 4.1. Ultrasonic data for Fe-18Cr-

12Ni-2Mo [Ledbetter 1981] were measured for polycrystalline samples. The bulk and shear modulus were measured with the ultrasonic method for polycrystalline samples of austenitic stainless steels. From them and using the empirical relation for the Zener anisotropy and C_{12}/C_{11} two sets of elastic constants were obtained. From these two sets of elastic constants mean values were calculated. [Kim 1994] use the assumption, that the elastic moduli of Fe-Cr-Ni-Mn can be written as a linear combination of the chemical composition. In both systems elastic constants were obtained using empirical relations [Ledbetter 1981] between elastic constants and moduli. These relations are defined by A=3.51 and the ratio C_{12}/C_{11}=0.635. When only a first neighbour interaction A=2 exists, the resulting higher value of the Zener anisotropy gives an indication of lower mechanical stability. For different fcc systems the Zener anisotropy is A=3.17±0.52. In addition, low q fit of all 7 branches of the dispersion curves were used to obtain the elastic constants(table 4.1). As a criterion of the linear parts of the dispersion curves in which the difference between the gradient of the same dispersion curves in the long wave approximation and the model of the dispersion curves differs less than 10% is used . Using this relation and applying a least squares method to all dispersion curves the elastic constants C_{11}, C_{12} and C_{44} were calculated (table 2.2.2). To verify these empirical relations only a few single crystal studies exist. One of these studies was performed by [Ledbetter 1984] for the austenitic stainless steel Fe-19Cr-10Ni, which is very similar to the steel AISI-304(American Iron and Steel Institute) . From this we could see that the empirical relations for Zener anisotropy and C_{12}/C_{11} are working well also in this system. The reason why only so few ultrasonic studies on monocrystals exist is connected to the extreme technical difficulties due to the preparation of samples.

4.3   Density of states

The phonon density of states was measured with a time-of-flight spectrometer on polycrystalline samples. These data were compared with the density of states derived from force constants using the Born-von Karman model.

4.3.1   Experiment

The measurements[3] of the phonon density of states have been performed at the time-of-flight spectrometer DIN-2PI at the JINR(Joint Institute for Nuclear research), Dubna. This spectrometer works in direct geometry. Monochromatisation was realized by a chopper wheel. Polycrystalline plates of $10 \times 18 \times 65$ mm^3 (Fe-18Cr-16Ni-10Mn), $2\times 150 \times 150$ mm^3 (Fe-18Cr-12Ni-2Mo) and $12\times12\times2$ mm^3 (Fe-18Cr-10Ni) have been investigated using an incident neutron energy of of 10.3 meV. The range of momentum transfer was Q= 1.1-4.1 Å^{-1} for elastic scattering. The energy transfer, $\hbar\omega$, was measured in the interval 4-60 meV. The raw data were corrected for background and detector efficiency. In the low

---

[3]experiments were performed by Markus Hölzel

energy region background is much lower than signal from the sample. Averaging over a few channels is recommended in order to obtain a reasonable background correction.

4.3.2 Results

The phonon density of states for all 3 steels(Fe-18Cr-16Ni-10Mn, Fe-18Cr-12Ni-2Mo and Fe-18Cr-10Ni) show a typical behaviour of fcc systems: it has two peaks corresponding to the transversal and longitudinal mode. The multiphonon contribution is low, except in the high energy region, and therefore our procedure for multiphonon correction is valid. The phonon density of states for all 3 steels are very similar, only minor differences in the intensity of the longitudinal modes exist.
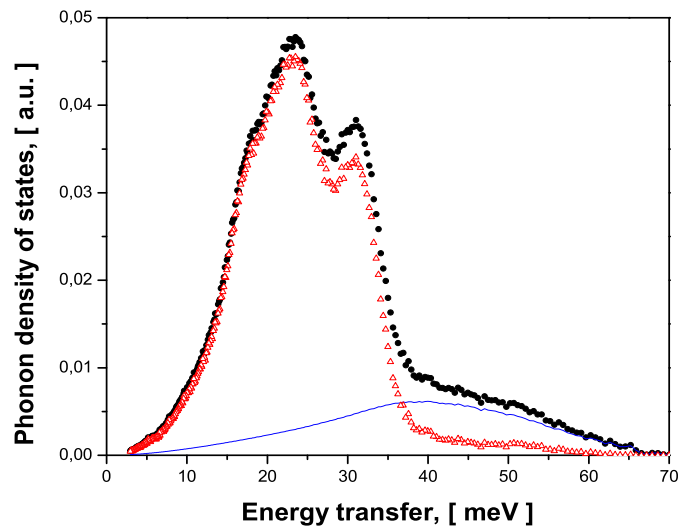

Figure 4.4: Phonon density of states for austenitic stainless steel Fe-18Ni-16Cr-10Mn, (•) experimental data, (—) multiphonon contribution and (△) DOS after multiphonon correction, $< u_\alpha^2 >$=0.00392 $\mathring{A}^2$.